JGR Atmospheres

RESEARCH ARTICLE
10.1029/2020JD033748

The Impact of Föhn Conditions Across the Antarctic Peninsula on Local Meteorology Based on AWS Measurements

Amélie Kirchgaessner[1], **John C. King**[1], **and Philip S. Anderson**[2]

[1]Atmosphere, Ice and Climate, British Antarctic Survey, Cambridge, UK, [2]Marine Technology, Scottish Association for Marine Science, Oban, UK

Key Points:

- Föhn-compatible signatures seen in record from an AWS just to the east of the Antarctic Peninsula mountains
- Strong Föhn signature in relative humidity in all seasons, while Föhn signature in air temperature depends on season
- Föhn can raise air temperature above freezing point at all times of year

Supporting Information:

- Supporting Information S1

Correspondence to:

A. Kirchgaessner,
amelie.kirchgaessner@bas.ac.uk

Citation:

Kirchgaessner, A., King, J. C., & Anderson, P. S. (2021). The impact of Föhn conditions across the Antarctic Peninsula on local meteorology based on AWS measurements. *Journal of Geophysical Research: Atmospheres*, *126*, e2020JD033748. https://doi.org/10.1029/2020JD033748

Received 21 AUG 2020
Accepted 17 JAN 2021

Abstract Föhn winds are warm, strong, downslope winds on the lee side of mountains, which can last from several hours to a few days. Recently Föhn conditions over the ice shelves on the eastern side of the Antarctic Peninsula (AP) mountains have attracted particular interest in the polar science community. Here, on the Larsen ice shelves (LIS) they provide atmospheric conditions for significant warming over the ice shelf which are thought to have clearly contributed to the collapse of Larsen A and B ice shelves in 1995 and 2002, respectively. We examine the representation of Föhn conditions as observed by measurements at an Automatic Weather Station (AWS) located on Cole Peninsula (CP) on the east of the AP mountain range in 2011. We introduce criteria to identify Föhn conditions and analyze the meteorological conditions at the AWS location with regard to the influence of Föhn overall, and on a seasonal and monthly basis. We consult two cases to highlight the seasonally different effects Föhn can have. We also compare our findings with data obtained in other studies, e.g., an AWS in a comparable location at Flask Glacier (FG). Measurements obtained at a crest AWS on the Avery Plateau (AV), and the analysis of conditions upstream using the Froude number help to put observations at CP into a wider context. Most importantly our data show that Föhn conditions can raise the air temperature to above freezing, and thus trigger melt/sublimation even in winter.

1. Introduction

In the second half of the 20th century, the Western AP has been one of the most rapidly warming parts of the planet, with the largest warming occurring in the winter season (King et al., 2003; Turner et al., 2005; Vaughan et al., 2001). These different studies find warming rates that are 1 order of magnitude bigger than the mean rate of global warming as reported by the Intergovernmental Panel on Climate Change (IPCC, 2007). Looking in more spatial detail, though, Marshall et al. (2006) found that between 1965 and 2000 rapid regional summer warming had occurred on the east coast of the northern AP, with near-surface temperatures increasing by more than 2 K over the period. The years from 2000 to 2014, in which this study falls, though, have displayed a cooling trend in this region (Turner et al., 2016).

The weather and climate of the AP are strongly influenced by the pattern of pressure variability between central Antarctica and the midlatitudes. This pressure pattern is referred to as the Southern Annular Mode (SAM). It drives the circumpolar westerly winds that dominate the Southern Ocean around the Antarctic continent, and determines their strength. Since approximately 1965 the SAM has exhibited a distinct trend to a more positive polarity, thought to be a consequence of anthropogenic forcing (Marshall, 2003).

In line with this trend to a more positive index of the SAM, the mean geopotential height over Antarctica has decreased, which in turn has strengthened the circumpolar vortex and thus the circumpolar westerlies (Marshall, 2004). These winds only encounter one topographic barrier in their way, which is formed by the mountain range that runs along the entire length of the AP. This, with its peaks of over 2,000-m height and its north-south orientation, forms a very effective barrier for the circumpolar westerlies around the Antarctic continent (Figure 1).

Marshall et al. (2002) find that surface warming in the region of the AP is substantially greater than that higher up in the troposphere, which casts doubt on the theory that atmospheric circulation is responsible for the warming. Orr et al. (2004) proposed a "low level" orographic explanation for the warming of the western

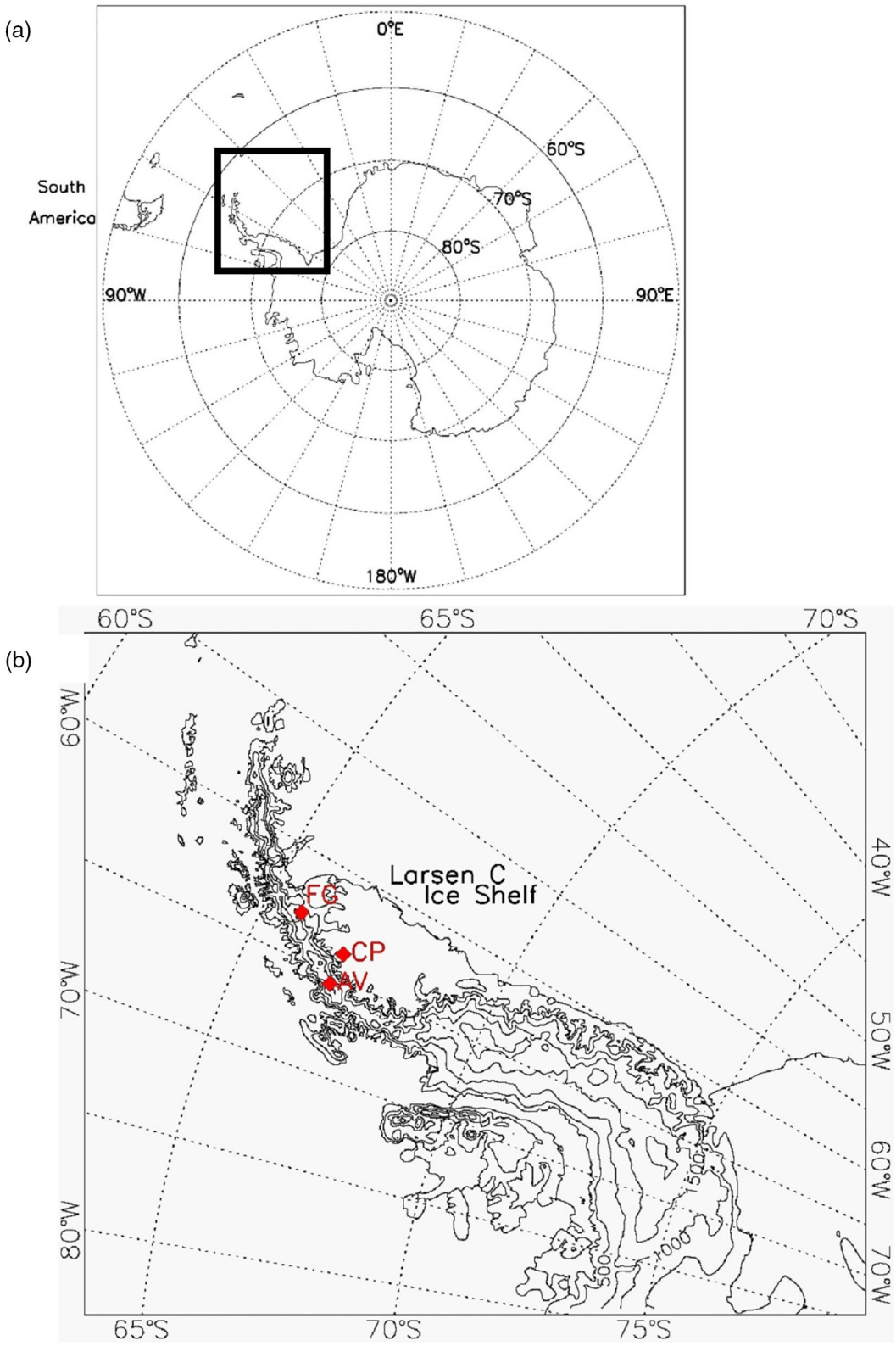

Figure 1. Map of Antarctica (a), and the Antarctic Peninsula (AP) (b), showing the locations of the weather stations at Cole Peninsula (CP), Flask Glacier (FG), and Avery Plateau (AV) (red diamonds), and of the Larsen ice shelf. Contour lines of the orography of the AP have been drawn at 500-m intervals.

AP, whereby the oncoming westerlies are blocked and deflected southwards by the AP mountains, giving rise to increased northerlies and enhanced advection of warm air into the area. Marshall et al. (2006) went on to identify a strong correlation between the considerable summer surface warming on the east side of the AP and the positive trend in the SAM, which is most apparent during summer (Marshall, 2003). A regional mechanism to explain this relationship was proposed in the form of so-called Föhn winds. Föhn winds are regional warm winds on the lee side of mountains. They occur frequently, e.g., on the northern side of the European Alps (Hann, 1885) or the eastern slopes of the Rocky Mountains (Whiteman, 2000). In this particular case, the increasing westerlies drive enhanced air flow over the AP, thus inducing strong lee side downslope winds and adiabatic warming on the east side (Elvidge et al., 2016). Indeed Cape et al. (2015) find that the positive trend in SAM is reflected in a significant increase of Föhn days in summer (days experiencing six or more hours of Föhn conditions) in the northeastern part of the AP.

Two main mechanisms lead to Föhn events. First, thermodynamically driven Föhn in a linear flow regime, e.g., when strong westerlies drive warm moist air from the (mostly) ice-free ocean up the western slopes of the AP mountain range. The rising air undergoes adiabatic expansion and cools, and eventually reaches saturation point. Subsequent condensation and precipitation remove moisture and leads to irreversible loss of latent heat (Beran, 1967; Smith, 1990). Model results by van Lipzig et al. (2008) reflect this with increased cloud cover, surface mass balance (which correlates with precipitation), and cloud ice/water to the west of the AP during periods of positive SAM (SAM+) conditions, i.e., stronger westerly circumpolar winds. Upon reaching the brow of the AP, the air, denser than its surroundings, sinks and undergoes adiabatic compression heating. The resultant air on the lee side is warmer and drier than that on the windward side (Orr et al., 2008). Second, Föhn caused through isentropic drawdown in a nonlinear flow regime, i.e., when air is sourced from higher altitude upwind of the obstacle as a result of upwind flow blocking at a level below the ridge crest. In a stably stratified atmosphere, this air will be potentially warmer and usually drier than the air below (Richner & Hächler, 2013; Smith, 1990). In both cases mechanical mixing and radiative heating can additionally lead to a warmer, drier air at low level (Elvidge & Renfrew, 2016; Ólafsson, 2005).

Warm, dry Föhn in the lee of the AP can lead to periods of melt over the Larsen C ice shelf (LCIS). These initially lead to firn densification and subsequently provide the melt water for hydrofracturing (Cape et al., 2015; Kuipers Munneke et al., 2014; McGrath et al., 2012). Hydrofracturing, i.e., the widening of crevasses due to the excess hydrostatic pressure exerted by intruding meltwater accumulating in crevasses, is generally accepted as the mechanism behind the dramatic collapse and break-up of Larsen A and Larsen B ice shelves in 1995 and 2002, respectively (Banwell et al., 2013; Scambos et al., 2003).

Using one year of observations from an Automatic Weather Station (AWS) at the eastern foot of the AP mountains we investigate the frequency with which Föhn events are observed at this location, and how they manifest themselves in the observational data, particularly in comparison to non-Föhn situations. Analyzing them in the context of regional meteorological patterns allows us to connect them to other data sets that are either more readily available or go back further in time, e.g., observations on the South Shetland Islands, or model output from the European Centre for Medium Range Weather Forecast (ECMWF) reanalysis data sets.

Previous studies investigating Föhn in the region of the Larsen ice shelves based on observational data have mostly concentrated on individual cases or seasons (Elvidge et al., 2015; King et al., 2017; Kuipers Munneke et al., 2012; Turton et al., 2017). Exceptions to this are recent papers by Turton et al. (2018) and Cape et al. (2015). While Turton et al. (2018) present a mini climatology of strength, distribution and propagation of Föhn over the LCIS based on observations and model output, they do not look into the details at individual locations, or put Föhn over the LCIS into a regional context. Cape et al. (2015) concentrate in their work on one main set of observations, with a focus on the remnants of Larsen A and B ice shelves. In a recent paper which uses some of the same AWS data as this study, Kirchgaessner et al. (2019) investigated how well Föhn conditions on LCIS are represented in a regional weather forecasting model. They found that the main characteristics of Föhn, high temperature and low humidity are underestimated. In this paper, we put observations of Föhn on the LCIS (CP) into a wider context by analyzing the conditions on the windward side and on the spine of the AP during Föhn.

2. Data and Methods

This study concentrates on the central part of the AP, where Föhn winds crossing the AP mountains have the potential to contribute to surface melt on the LCIS, the largest remaining ice shelf on the eastern side of the AP. The coastline in the region of the LCIS is a sequence of jagged peninsulas and inlets, Cole Peninsula (CP) being one of them. To the west of the ice shelf the terrain quickly rises up to the Avery and Bruce Plateaus, which reach heights of 1,700 m above sea level and more. FG is one of the many glaciers that drain from Bruce Plateau eastwards. It feeds into Scar Inlet, just to the north of LCIS (Figure 1).

The main data source for this study is an AWS on CP. This was the first AWS to be installed in the region close to the foot of the AP mountains, which is strongly affected by Föhn. To put the characteristic of these observations into a wider context, we compare the observations to those from an AWS at FG. We consult data from a third AWS on the crest of the AP on the AV, and atmospheric model simulations from the Bellingshausen Sea, to analyze the flow conditions during Föhn events. As far as we are aware, the project OFCAP (Orographic Flows and the Climate of the Antarctic Peninsula) was the only time, when there was an AWS operating at the foot of the AP on the Larsen C ice shelf (CP) and another one on the crest of the AP (AV) at the same time.

2.1. Automatic Weather Station at Cole Peninsula

In this study, we make use of data from an Automatic Weather Station (AWS) that was deployed on the eastern side of the AP, on January 21, 2011. The AWS was located at 66°51′48″S, 63°48′39″W, 424 m above sea level on CP, a low snow-covered promontory extending eastwards from the foot of the main AP mountain chain (Figure 1). It was revisited for maintenance on December 14, 2011. About 0.5 m of snow had accumulated at the location between deployment and maintenance visit. Possibly due to intrusion of melt water, the AWS then stopped working reliably on January 4, 2012. The AWS measured wind speed (ff) and direction (dd) with a Young propeller-vane anemometer at ∼4 m, air temperature (T) and relative humidity (RH) with a Vaisala Humicap HMP45 at ∼3.5 m, and absolute air pressure (p) by microelectromechanical sensors, buried at the foot of the AWS. Measurements were logged at 0.1 Hz, from which 10 min mean values were calculated internally. These were stored on a separate memory card and transmitted back via Iridium satellite communication about every 12 h. The AWS data were averaged into 6-hourly values, to ensure that when Föhn is identified, they represent a significant period of time rather than just a short blip in the measurements. Centered averages were calculated for 3, 9, 15, and 21 UTC. Mean values of the wind direction were calculated by averaging the u-component and v-component of the wind direction. Values of RH were adjusted to saturation over ice for below-freezing temperatures. A more comprehensive description of the instrumentation and data collection of the AWS at CP can be found in Kirchgaessner et al. (2019).

The period under consideration in this study starts on January 22, 2011 and finishes at the end of the year on December 31, 2011. This includes 344 days of potential data, and—with regard to 6-hourly data used here—1,376 potential data points. Any gaps in the data set are clearly linked to the frequency with which data were sent back via satellite. At high latitudes such interruptions cannot be ruled out when no satellite is visible at the time of intended data transmission. All in all, <11 days of measurements are missing from data set used for this analysis.

2.2. Automatic Weather Station on Avery Plateau

The second AWS that we use in this study was deployed on the spine of the AP mountain range, in an area called the Avery Plateau (AV). It was deployed on January 9, 2011. Its exact location was 66°52′38″S, 65°27′23″W 1,813 m above sea level. In its design and instrumentation, it was identical to the one at CP. The spine of the AP is an area of high snow accumulation. Consequently, the station was eventually buried in snow. As the snow level reaches the T and RH sensors at ∼3.5 m, the fluctuations in their measurements are more and more dampened. Eventually, when the sensor is completely buried by snow the signal turns into a constant value. A few days later a similar change is apparent in the measurements by the propeller wind

vane at the top of the AWS at ~4 m. We use data until July 11, 2011. We have chosen this day, as it is the last day before a weather event that led to the first signs of the accumulating snow affecting the measurements. To our knowledge, these extremely difficult conditions make this 6 month long meteorological record from the spine of AP unique.

During westerly flow the AWS at AV is directly upstream of the AWS at CP.

2.3. Data From Flask Glacier

The station at FG was installed as part of the Automated Meteorology-Ice/Indigenous species-Geophysics Observation System (AMIGOS). It is located at 65°45′S, 62°53′W, and at 450 m asl (according to unavco.org: 582.60 m asl). Stations of this system are equipped with a Vaisala Weather transmitter WXT520, and measure T, p, RH, dd, and ff as well as precipitation. Data are usually collected every 5 min and transmitted as hourly data. FG data are available to download at http://www.unavco.org/ (Scambos & Truffer, 2010). FG and CP are at an approximate distance of 123 km, and roughly 100 km apart in north-south direction. Data for comparison are available from January 22, 2011, when measurements at CP begin until September 7, 2011, after which no data are available for 2011 from FG.

2.4. Antarctic Mesoscale Prediction System (AMPS)

In the absence of suitable observational data, we use model simulation by the Antarctic Mesoscale Prediction System (AMPS) in this study to analyze the flow upstream of the AP mountains. One potential source of observational data could be Rothera station, but it is not only too close to the AP, but it is during westerly flow it is in the lee of Adelaide Island. For these reasons, measurements from Rothera do not represent undisturbed upwind conditions. AMPS (Powers et al., 2012) is a numerical weather prediction (NWP) system for the Antarctic region, run operationally by the Mesoscale and Microscale Meteorology Division of the National Center for Atmospheric Research (NCAR) in Boulder, Colorado, USA. Forecasts are available through a web-based repository that provides support for the United States Antarctic Program, Antarctic science, and international Antarctic efforts (Powers et al., 2003). For the period under investigation, AMPS used the nonhydrostatic Weather Research and Forecasting model (WRF) v3.0.1 with modifications to improve the representation of the surface energy balance over permanently ice-covered regions. This model configuration is commonly referred to as Polar WRF (Hines & Bromwich, 2008; Skamarock et al., 2008). It is important to note that AMPS is primarily an operational forecast system and has not been optimized for research purposes, although it has proved of value as such in numerous studies, e.g., Hines et al. (2019), Turton et al. (2018), Wille et al. (2016), and Fogt and Bromwich (2008).

During the period under investigation, AMPS was run to cover a domain of 346 × 301 grid points in the region of the AP at a horizontal resolution of 5 km (Figure 1). Forecasts were run twice a day, starting from GFS analyzes valid at 0000 UTC and 1200 UTC. Forecasts for the 5 km AP domain were run to T + 36 h for each of these initialization times. After having served its purpose as a weather forecasting tool, the hourly model output is stored in the AMPS Archive. Through this archive, the data are subsequently available for the scientific community for studies like this present one, and are accessible on https://www.earthsystemgrid.org/.

A more detailed and comprehensive description of the Antarctic Mesoscale Prediction System, the underlying model and its setup and configuration for the period under investigation can be found in Kirchgaessner et al. (2019).

2.5. Identification of Föhn

Data points from CP and FG AWS data sets are classified as Föhn if they fulfill a certain set of criteria. These criteria have been developed by identifying potential Föhn events in the AWS data set. They are based on two main signatures of Föhn events: a sudden increase in temperature combined with a decrease in humidity. How T and RH are in antiphase during Föhn events can be seen clearly in Figure 2. The criteria that we use for Föhn are

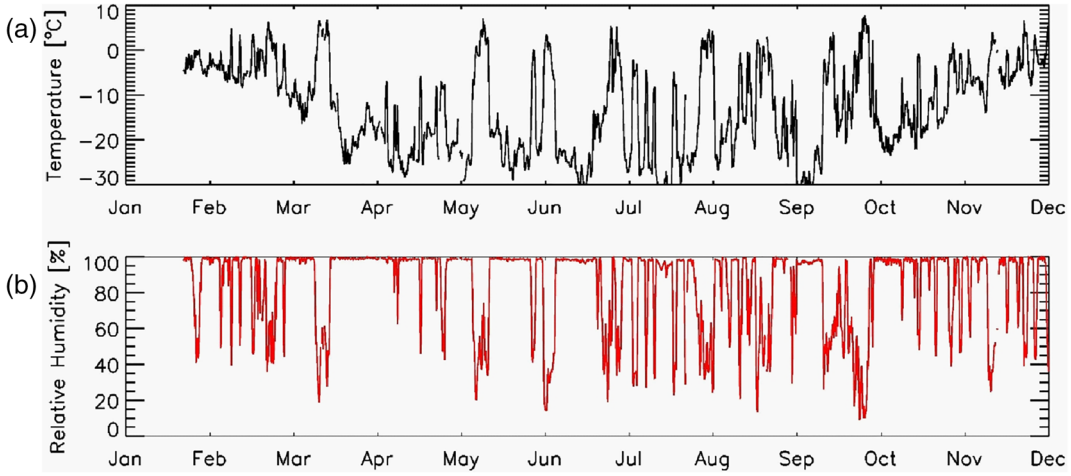

Figure 2. Time series of 6-hourly mean values of *T* (a) and RH (b) at CP AWS from January 22, 2011 to December 31, 2011. RH, relative humidity; AWS, Automatic Weather Station.

- RH lower than or equal to 65%

or

- RH lower than or equal to 70%

and

  - *T* increase in previous 12 h of 3 K or more

  or

  - *T* decrease of 3 K or more over the following 12 h

Similar criteria have been applied by other studies investigating Föhn in Antarctica (Speirs et al., 2010; Steinhoff et al., 2014) and elsewhere (Richner et al., 2006). While Speirs et al. (2010) and Steinhoff et al. (2014) base their identification on the rate of change of *T* and RH, their identification is based on 15 min measurements. Using averages over 6 h as in this study leads to comparable rates of change for both RH and *T*. Richner et al. (2006) use a very similar approach to the one used in this paper; a (semi-)automated Föhn diagnosis, based on a wind index which combines speed and directional information, together with anomalies of *T* and RH. The most obvious criterion for Föhn identification would of course be the presence of westerly wind. This has been shown to be a good indicator for Föhn in particular cases, e.g., in Kuipers Munneke et al. (2012) and Kuipers Munneke (2018), but was found to be unreliable in identifying Föhn conditions at CP in this data set. This is likely due to local influences on the wind direction at the AWS.

In parallel, the same period was scrutinized for Föhn events using AMPS data. This test looks for a drawdown of potential temperature contours (isentropes) on the lee side of the AP mountains. For this the potential temperature at the height of the mountain barrier in undisturbed conditions upwind of the AP at the latitude of CP is determined. This isentrope is then followed eastwards over the LCIS, to the longitude of its minimum height above sea level. If this drops below a threshold within 2° of the AP, we identify this situation as a Föhn event. This test is described in more detail in Kirchgaessner et al. (2019). This additional test was applied to exclude Föhn-like signals in the AWS signal that were caused by other circulation patterns, e.g., cyclones that form at the tip of the AP.

The two algorithms identify Föhn for 224 of the overall 1,352 data points at CP (6-hourly data from January 22, 2011 to December 31, 2011), and classify 774 data points as "no Föhn." On 354 occasions, the algorithms disagree in their assessment; these data points are kept in the pool of "all data" points for the general analysis of the meteorological conditions at CP. Kirchgaessner et al. (2019) have shown that overall both algorithms agree well in their identification. We can therefore be confident that this step does not skew our data against thermodynamically driven Föhn.

Table 1
Average Values and Standard Deviations of Standard Meteorological Parameters as Observed by the AWS at CP for All Data Points, and Calculated Separately for Föhn and no Föhn Data Points

	T (°C)	p (hPa)	RH (%)	u (m/s)	v (m/s)	ff (m/s)
All measurements (n = 1,352)	−12.2 ± 10.3	942.7 ± 11.9	84 ± 24	2.5 ± 3.1	0.4 ± 3.4	4.1 ± 3.3
No Föhn (n = 774)	−16.9 ± 8.8	942.9 ± 11.8	97 ± 5	2.9 ± 3.1	1.2 ± 3.1	4.2 ± 3.3
Föhn (n = 224)	−0.4 ± 5.0	943.4 ± 11.4	46 ± 13	1.4 ± 2.6	−1.9 ± 2.5	3.4 ± 2.7
Diff (Föhn − all)	11.8 K***	0.7 hPa	−38%***	−1.1 m/s***	−2.3 m/s***	−0.7 m/s***

All 224 data points that were classified as Föhn were additionally visually verified as such by determining large scale flow patterns based on ERA-Interim reanalysis fields of geopotential heights (Dee et al., 2011). This overall number of Föhn conditions corresponds to 16% of all data. Any individual data point to which Föhn criteria as described above do apply will be called a Föhn condition. A series of subsequent Föhn conditions will be called a Föhn event.

The same criteria were applied to the data from FG. This results in 101 of 916 data points being identified as Föhn. At CP 136 Föhn conditions were identified for the same period (i.e., between January 22 and September 7, 2011), although only 73 of these coincided with those observed at FG. Due to the spatial distance between the two AWS this is not surprising. As, e.g., Turton et al. (2018) show Föhn conditions often occur at different locations along the AP with a temporal offset or last longer at one location than at another. Several reasons either on their own or combined can cause this.

(1) Naturally the mountains along the AP differ in height. Depending on the strength of the flow, and the stratification upstream, overflow may only occur at lower sections of the AP mountains
(2) The strength of the westerly flow can vary zonally, i.e., Föhn may only occur where the flow is strongest
(3) the zonal location of this strongest part of the flow will change on synoptic time scales

3. Results

3.1. Mean Conditions at CP

Table 1 gives an overview of the general meteorological conditions at CP during the period under investigation. Mean values and standard deviations of T, p, RH, zonal and meridional wind components (u, v), and ff are presented for all data points, and separately for those that show Föhn and no Föhn conditions, respectively. The table also shows the mean difference between Föhn conditions and all conditions.

The average observed T at CP over the period under investigation was −12.2 °C, with temperatures varying between −36.6 °C in July and +7.8 °C in early October. This maximum occurs during a Föhn event.

RH during the entire period ranged from 10% to 100%. The minimum value was observed in early October during the same Föhn event that also led to the highest value in T.

We also analyzed the persistence of Föhn. Figure 3 shows that Föhn conditions mostly do not last longer than 6 h. The longest uninterrupted Föhn event, which lasted for 3.5 days, occurred in August. The median duration of Föhn events at both locations is 12 h.

3.2. Conditions at CP During Föhn

Overall 224 data points were classified as Föhn conditions. During these conditions, T, RH, ff, and wind components u and v during Föhn are all significantly different from the mean conditions (Table 1). There are some significant differences between conditions measured by the AWS during Föhn and no Föhn periods. The average T during no Föhn is −16.9 °C, rising to −0.4 °C during Föhn conditions. As Föhn conditions occur throughout the year, T values close to and above freezing can occur during Föhn in all seasons.

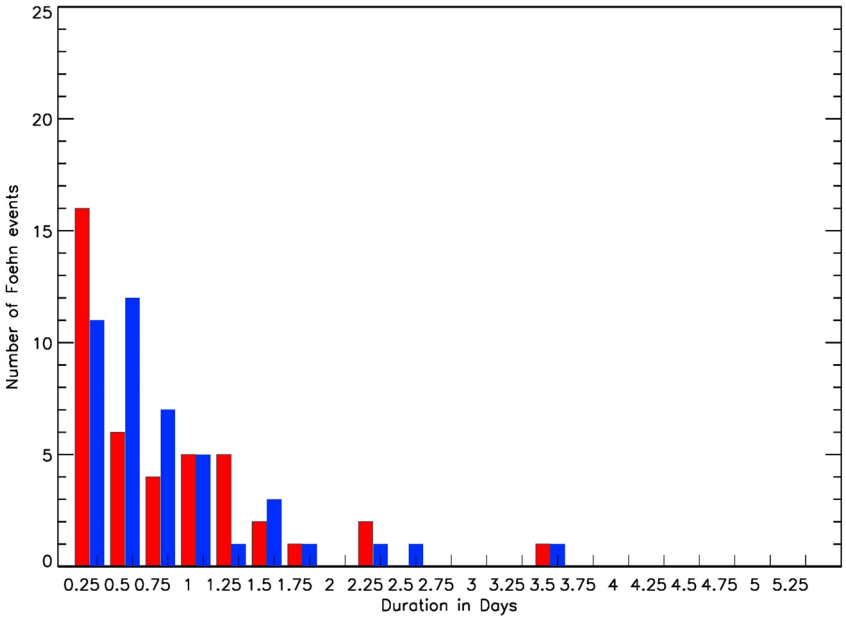

Figure 3. Duration of Föhn episodes in fractions of days. Blue: Flask Glacier AWS, red: Cole Peninsula AWS. AWS, Automatic Weather Station.

Due to the generally cold climate, the atmosphere in Antarctica in absolute terms is extremely dry. Large differences in RH therefore reflect small changes in absolute humidity. In the observational data the mean difference in RH between Föhn and no Föhn is 51%, with RH being close to saturation at 97% on average during no Föhn, and significantly lower at 46% on average during Föhn. The small standard deviations for both conditions show the clear separation in RH between Föhn and no Föhn. This justifies its use in Föhn identification. It also indicates that the chosen way to identify Föhn is robust, and should be fairly insensitive to the chosen RH thresholds.

The values in Table 1 indicate that we observe on average southwesterly winds at the AWS generally and during no Föhn times, and northwesterly wind during Föhn. A more detailed look at ff and dd is presented in panels (a) and (b) of Figure 4. During no Föhn, the wind comes from the southwest for 40% of the time. For Föhn cases, the wind comes predominately from the north, although dd is generally more varied during Föhn than during no Föhn, and the wind can come from all sectors between northeast and southwest. The average value of ff differs significantly between all cases and Föhn cases. Significant differences in the u-component and v-component of the wind reflect the changes in dd mentioned above. The average ff during Föhn events is not only significantly smaller than that during no Föhn conditions, but also than the general average at the AWS.

Regarding T and RH these findings agree well with the expected signal during Föhn of warmer and drier air masses. Somewhat counterintuitively, we observe a statistically significant reduction of the westerly (u) component of the wind during Föhn.

Figure 5 shows the monthly percentage of 6-hourly data points that were identified as Föhn at CP and FG. The January figure for CP may not be representative for the month as a whole, as measurements only began on the 22nd of the month. The minimum frequency at CP is seen in April (7, <6%), the maximum in August with 37 out of 124 data points (>29%) classified as Föhn. While the overall length of the data set is not sufficient for a statement about seasonal differences, it is clear that Föhn conditions can occur throughout the year. This distribution does not differ much between CP and FG. The main differences occur in June and July, with a slightly higher percentage of Föhn at CP in June and a slightly higher percentage of Föhn at FG in July. The high percentage of Föhn at FG in September is caused by the unavailability of data at FG after September 7. With a major Föhn event at the beginning of the month this leads to a high percentage of Föhn at FG in this particular month. The results also agree well with the finding

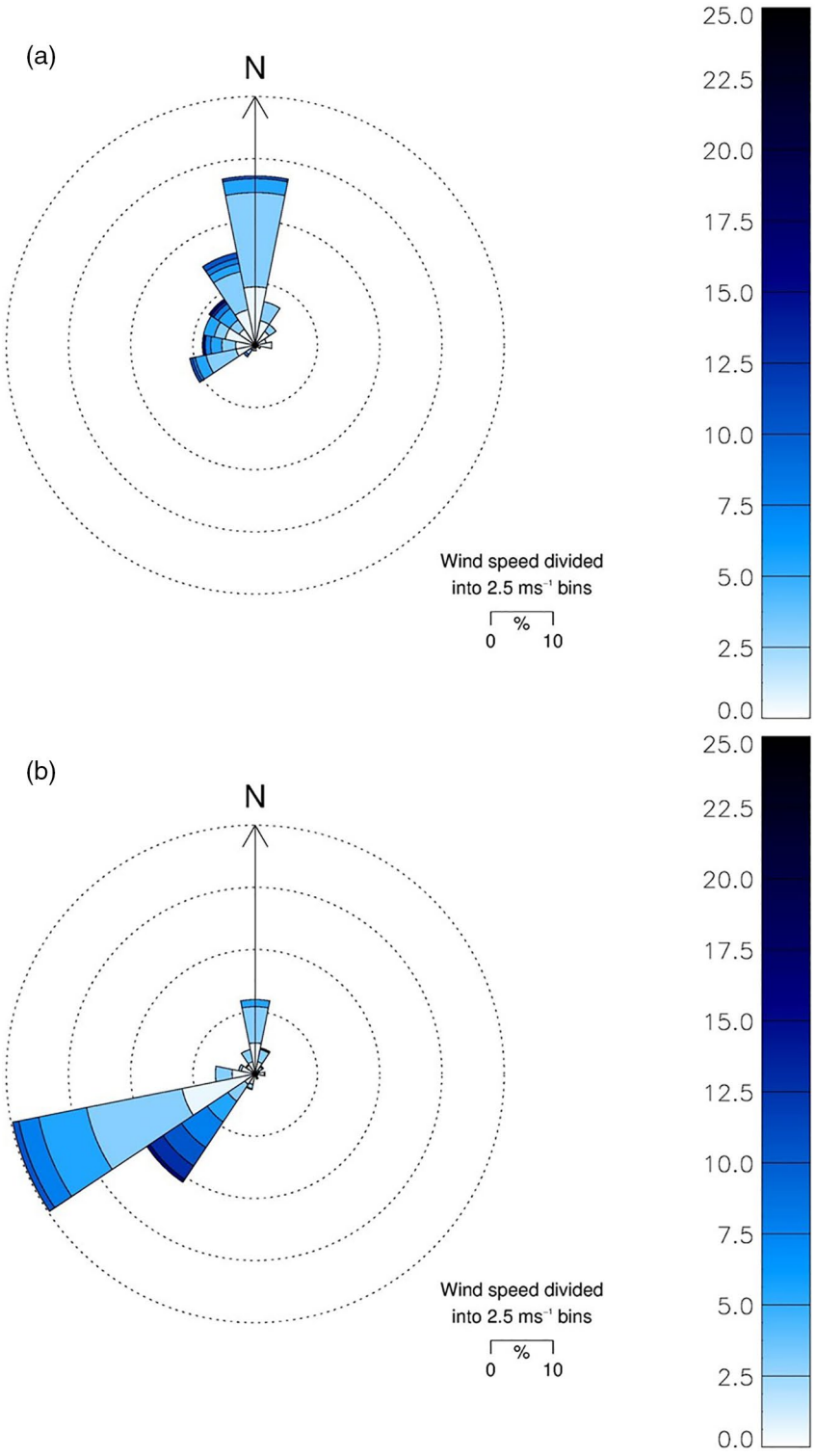

Figure 4. Wind roses based on measurements at Cole Peninsula for non-Föhn conditions (a) and Föhn conditions (b).

by Cape et al. (2015) who showed that the largest positive temperature trend between 1962 and 2010 was observed in the winter months of June, July, and August. While there have not been that many Föhn events during the winter months in this particular year, our results show that Föhn conditions have the

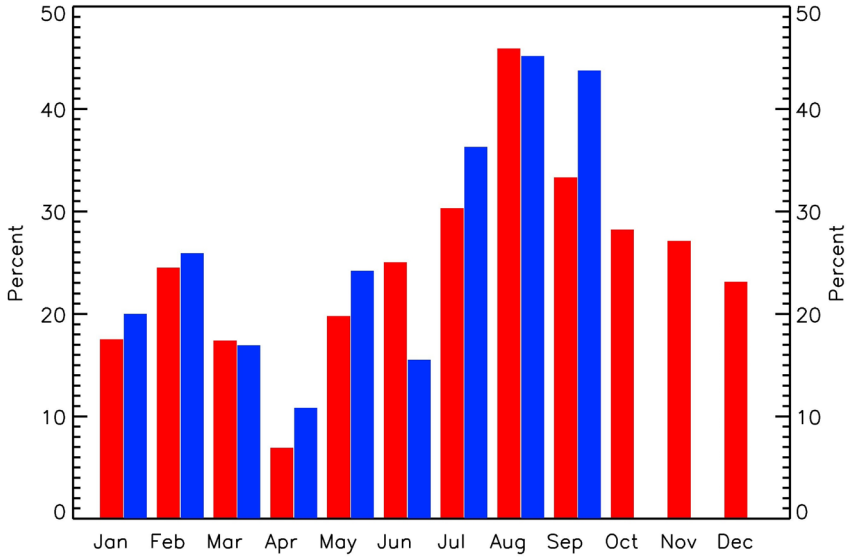

Figure 5. Relative number of six-hour Föhn conditions in each calendar month of 2011. Blue: Flask Glacier AWS, red: Cole Peninsula AWS. Flask Glacier AWS ceased operating after September 2011. AWS, Automatic Weather Station.

potential to contribute to this significant trend through rapid temperature increases of 20 K, and to above freezing air temperature. Such extremely high temperatures occur in winter only during Föhn events. This is especially relevant as Föhn events are likely to increase in frequency with a shift to a more positive SAM in the future (Marshall, 2003, 2004).

3.3. Seasonal Differences

Figure 2 shows *T* and RH over the entire period of measurements in 2011. The plot shows clearly that (a) Föhn events occur throughout the year and (b) that *T* and RH during Föhn events do not differ greatly throughout the seasons.

Table 2 lists the seasonal anomalies in *T*, RH, *u*, *v*, and ff during Föhn compared to all data points. Asterisks mark the level of significance. We see that in all four seasons *T* during Föhn is significantly higher than under average conditions, particularly in autumn and winter, when "normal" temperatures are lower than the annual average. Anomalies in RH are very similar throughout the year. A prolonged period of Föhn in May may be responsible for the especially large seasonal *T* and RH anomalies in autumn of 2011.

Figure 6 shows monthly mean values at CP of *T* and RH for all data points, and for those classified as Föhn and as no Föhn, respectively. The significant influence that Föhn events have on *T* and RH in all months is visible in both graphs. An annual cycle is discernible in the monthly mean temperature of all data points, and no Föhn data points, as one would expect. The plot, however, also shows, that this annual cycle disappears almost completely for Föhn data points. This graph shows only slightly higher temperatures during summer months, while during the rest of the year the average temperature for Föhn seems to depend more on the duration and strength of the Föhn, which is often dependent on the persistence of the weather situation.

RH is very homogenous throughout the year, with Föhn events modulating its level. Due to the low temperature in the region, and thus a low saturation pressure, RH—measured above a snow surface—is generally close to saturation with respect to ice during no Föhn, and significantly lower during Föhn.

Table 2
Seasonal Mean Values of Anomalies in T, RH, u, v, and ff at CP During Föhn

	T (K)	RH (%)	*u* (m/s)	*v* (m/s)	ff (m/s)
DJF	4.99***	−34.79***	0.76*	2.24***	0.42
MAM	16.99***	45.17***	−1.32**	−3.18***	−0.88*
JJA	14.35***	34.48***	−0.97**	−1.15**	−1.02**
SON	10.17***	34.44***	−1.09**	−2.89***	−0.41

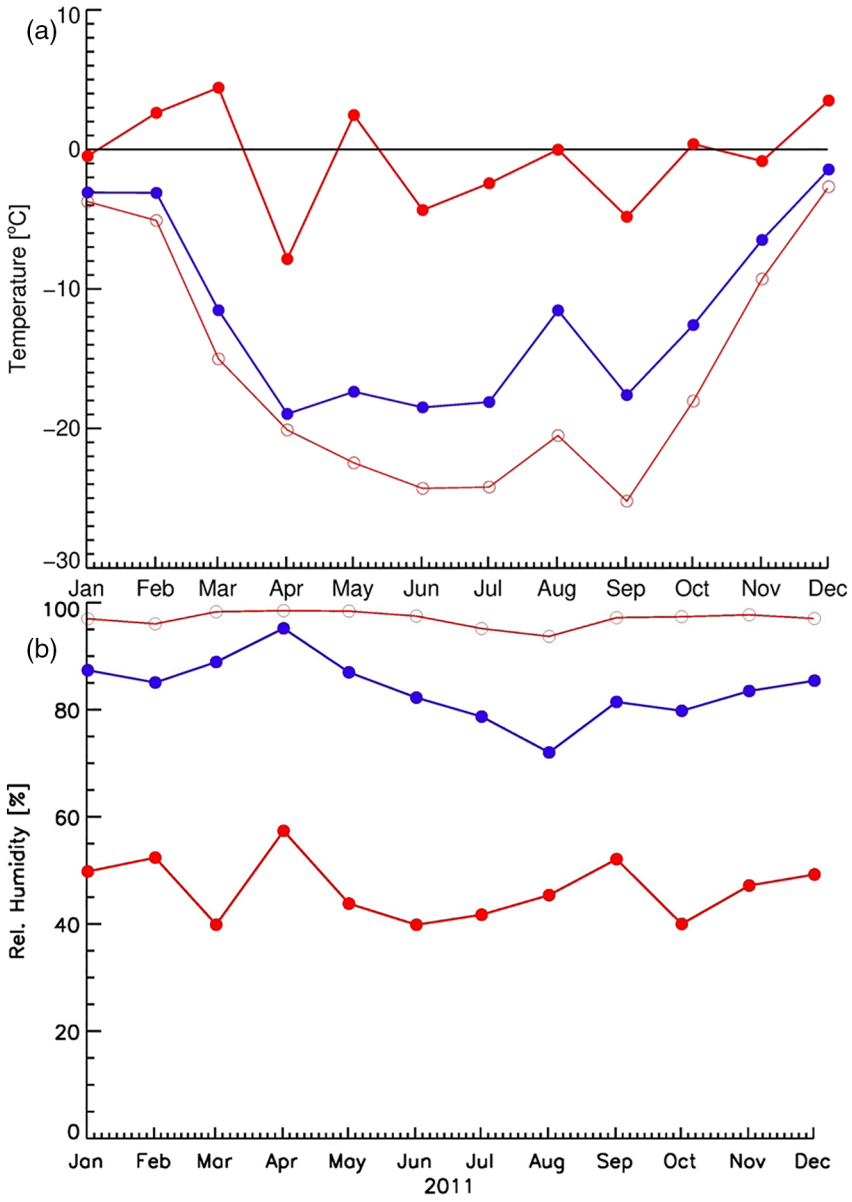

Figure 6. Monthly mean *T* (a) and RH (b) at CP for all data (blue), and separated into Föhn (red, filled circles) and non-Föhn (red, open circles) composites. RH, relative humidity.

3.4. Two Case Studies

We have examined two cases of Föhn occurrence in greater detail, one in February (case "a") and one in August (case "b") of 2011. Mean sea level pressure and near-surface wind field from the operational ECMWF forecast is shown in Figure 7 to present the defining synoptic scale situation for both cases. In case "a," a deep low-pressure system with a central pressure of 956 hPa was positioned at ~67°S, 76°W on February 24, 2011. This led to a northwesterly wind direction and very high ff of up to 24 m/s on the windward side of the AP. This pressure system had deepened by 22 hPa over the previous 24 h and had moved rapidly from the Amundsen Sea into this location. It then filled over the coming days, while a new strong low-pressure system over the Amundsen Sea gained dominance.

During case "b" a high-pressure system with a central pressure of 1,024 hPa, centered around 60°S, 70°W, forced a strong westerly wind across the AP and onto the LCIS. Over the next days, it moved further east and

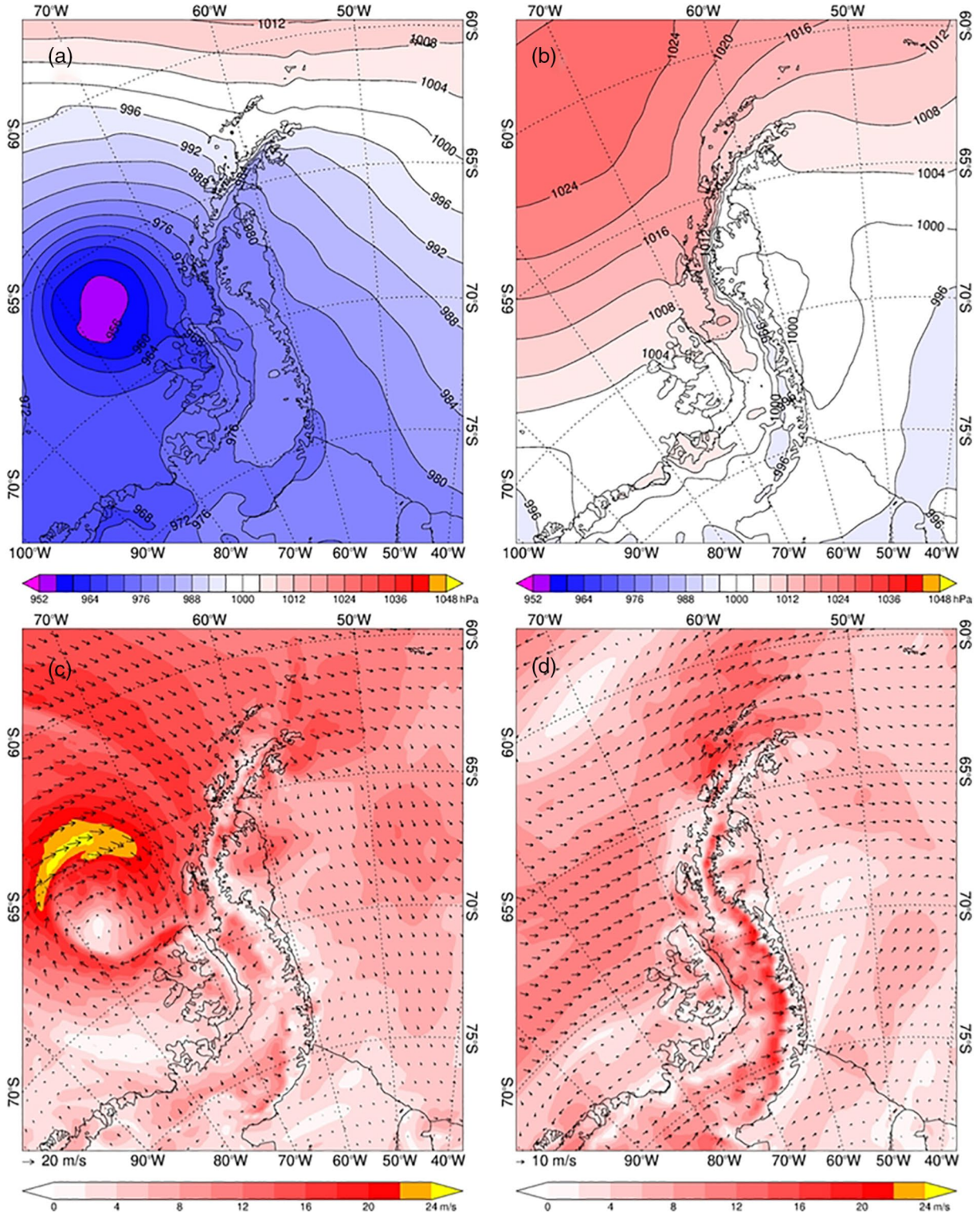

Figure 7. Mean sea level pressure (hPa) (a), (b) and 10-m wind field (c), (d) for February 24, 2011, 00 UTC (case "a," panels a and c), and August 8, 2011, 00 UTC (case "b," panels b and d) as forecast by the ECMWF operational model.

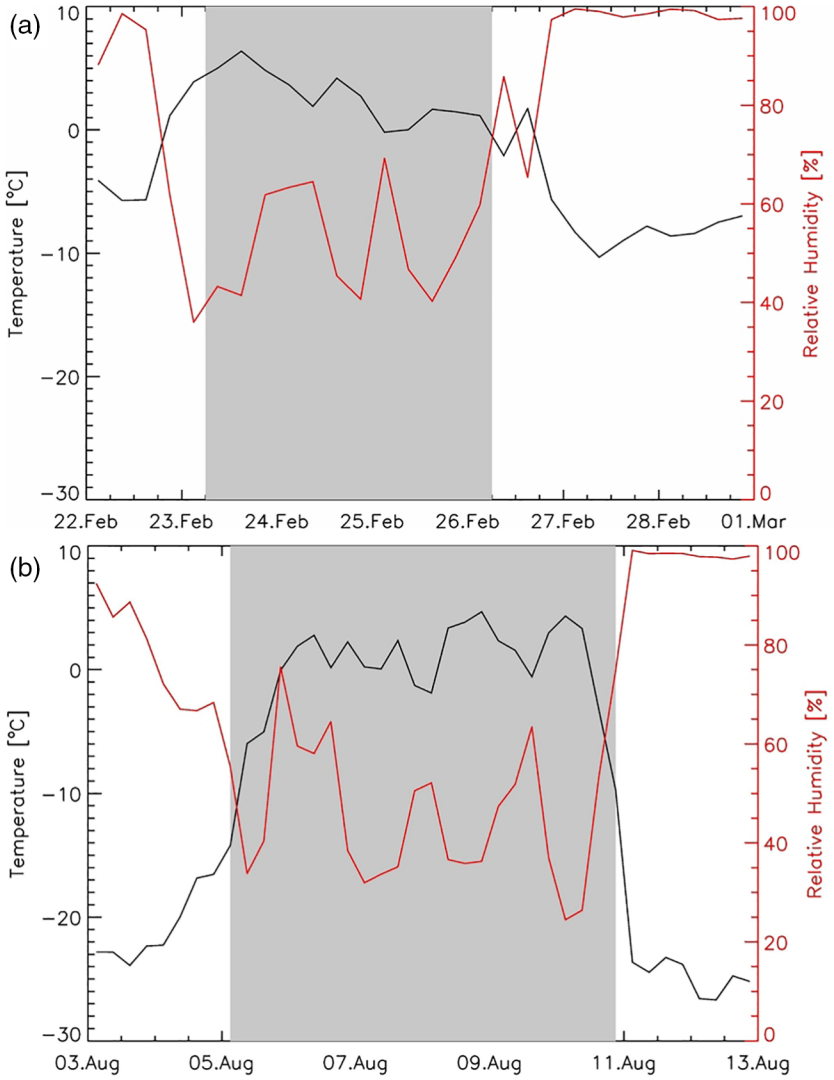

Figure 8. Temperature (black) and relative humidity (red) during Föhn in February (a) and August (b) 2011 as measured at CP. The areas shaded in gray are the periods identified as Föhn events according to the criteria set out in Section 2.5.

slightly further north, but kept its strength and remained the dominant synoptic-scale feature in the region. A low pressure that developed over the Amundsen Sea further strengthened the westerly wind regime in the region of the LCIS. Unlike in case "a," this low-pressure system then moved due north, bringing the westerly wind regime and thus the Föhn to an end.

Figure 8 shows *T* (black) and RH (red) during these 2 Föhn events. The comparison shows particularly in February that the Föhn signal in RH is far more pronounced than in *T*. While the temperature increase due to Föhn in February is about 3 K, which at that time of year is of a similar magnitude to temperature variations due to synoptic scale changes, the air temperature in the August case reaches a similar level as that in February, but from a far lower base line. RH though shows significant decreases in both cases. This comparison exemplifies why a decrease in RH below a certain threshold was used as the primary criterion for the identification of Föhn events rather than a temperature increase.

To investigate the flow regimes during the two case studies, we obtained back trajectories for near-surface air using the National Oceanic and Atmospheric Administration (NOAA) HYbrid Single-Particle Lagrangian Integrated Trajectory (HYSPLIT 4.0) model (Draxler & Hess, 1998). The patterns look very similar for

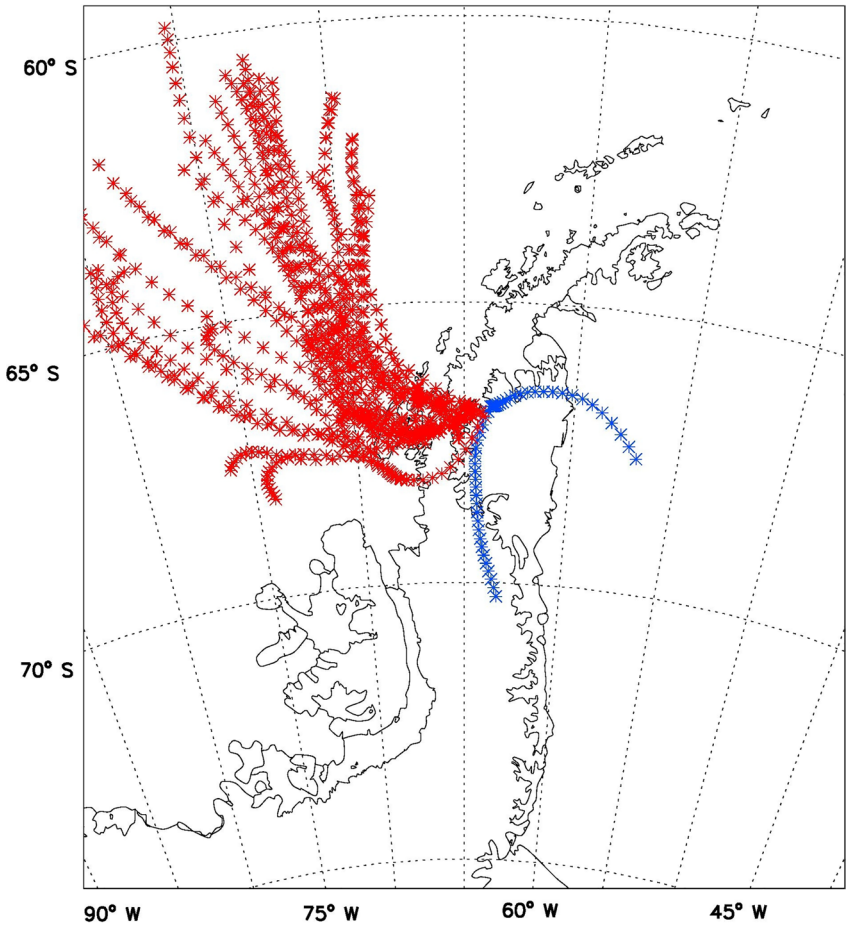

Figure 9. Back trajectories for the Föhn episode in August 2011, calculated with HYSPLIT using ERA-Interim as input data. In addition to trajectories during Föhn (red), trajectories 24 h before and after the Föhn episode are shown in blue. HYSPLIT, HYbrid Single-Particle Lagrangian Integrated Trajectory.

both cases though, and we only show back trajectories for the August case in Figure 9. The air masses arriving at the AWS during Föhn quite clearly originate from the windward side of the AP while the "before" and "after" trajectories in blue both show air masses originating to the east of the AP.

4. Wider Context

In this section, we examine the wider context of the findings laid out in the previous sections by using additional data sets to connect the local Föhn phenomena to large scale atmospheric circulation patterns beyond the AP and the Antarctic continent. First, we compare our findings from CP with data from an AWS at FG, situated in a similar setting, but 100 km further north. Second, we analyze data from an AWS on AV, directly upstream of CP on the spine of the AP. Lastly, we use the data from the AMPS archive on the windward side of the AP to calculate the Froude number as a means to characterize the flow conditions during the different Föhn events.

4.1. Comparison With Flask Glacier

Data from a weather station on FG were one of the data sets used in Cape et al. (2015) for their analysis of Föhn in the region.

We have applied the same Föhn identification criteria at both stations. Of 916 common data points, both stations agree on 825 occasions on the occurrence of Föhn (73) and no Föhn (752), respectively. This is

Table 3
Conditions at Flask Glacier and Cole Peninsula During the Period From January 22 to September 7, 2011 and for Föhn and no Föhn

	All measurements			Föhn		No Föhn	
	p (hPa)	T (°C)	RH (%)	T (°C)	RH (%)	T (°C)	RH (%)
Flask Glacier	925.5 ± 11.3	−14.0 ± 9.6	76 ± 13	−2.1 ± 3.9	56.1 ± 5	−16.4 ± 8.6	78.9 ± 11
Cole Peninsula	945.3 ± 11.6	−13.9 ± 10.3	76 ± 18	+1.2 ± 3.1	45.0 ± 13	−16.6 ± 9	80.2 ± 14

equivalent to 90% of all common data points. CP shows a Föhn signal about 25% of the time, and FG about 11% of the time. That there is a proportion of cases which is only captured by one and not the other, is easily explicable by their spatial separation, in particular their north-south distance.

Here, we compare data from CP to the FG data, as they are not only both on the lee of the AP, but also at a similar height above the LCIS. The reader should note, though, that the AP mountain range is about 200–300 m lower upwind of FG than upwind of CP. The values are compiled in Table 3. On average p is lower at FG than at CP, but T and RH are very similar. This similarity is reflected in the correlation between the two data sets of 0.99 (p), 0.89 (T), and 0.66 (RH) based on 6-hourly data. In 2011, data are missing from the FG record after September 7, which explains why mean meteorological values differ from those given for CP in Table 1. This means that the warmer months with higher RH from October to December (spring and early summer) cannot be considered in this comparison.

During non-Föhn conditions, T is on average higher, and RH is on average lower at FG than at CP (Table 3). Values of meteorological parameters during Föhn events indicate that Föhn is generally weaker at FG than at CP, i.e., less warm and less dry. This is in contrast to Turton et al. (2018) who analyzed data from six AWS on the lee side of the AP (including CP but not FG). They found a north-south gradient in the strength of Föhn events with Föhn being weaker the further south they were observed. As overall average conditions are very similar at FG and CP, it seems unlikely that the application of Föhn criteria developed for CP should exclude Föhn events at FG, and thus artificially weaken the Föhn signal in this comparison. It is likely though that this relative weakness of Föhn at FG is in part due to the fact that the AP mountain range is lower at the latitude of FG.

4.2. Conditions at the AV AWS During Föhn

In Table 4, we compare meteorological conditions at AV at times when Föhn and no Föhn conditions were observed at CP. Recall that, during westerly flow associated with Föhn events, AV is upwind of CP and is sampling air at the summit of the AP ridge that will subsequently descend toward CP.

All meteorological variables, apart from relative humidity, differ significantly between Föhn and no Föhn cases.

Critical for all these differences seems to be the extreme difference in dd and ff (Figure 10). The ff value is twice as high during Föhn than during no Föhn. During Föhn the wind comes predominantly from the northwest, while it generally comes from the south during no Föhn. Northwesterly wind at AV will most of the time originate from mostly ice-free open water to the west of the AP, while air arriving with southerly wind will arrive from snow and ice-covered regions of the AP and the Antarctic continent itself.

Table 4
Average Values and Standard Deviations of Meteorological Parameters as Observed at AV AWS During Periods When Föhn (Top) and no Föhn (Middle) Were Observed at CP

	T (°C)	p (hPa)	RH (%)	u (m/s)	v (m/s)	ff (m/s)	dd (°)
Föhn (n = 84)	−11.7 ± 4.8	789.8 ± 10.4	98 ± 8	7.3 ± 3.4	−4.1 ± 4.9	9.5 ± 4.3	299
no Föhn (n = 406)	−14.8 ± 5.6	783.1 ± 8.8	98 ± 7	0.1 ± 3.7	0.9 ± 4.0	4.9 ± 2.9	184
Difference	3.1**	6.7***	0	7.2***	−5***	4.6***	

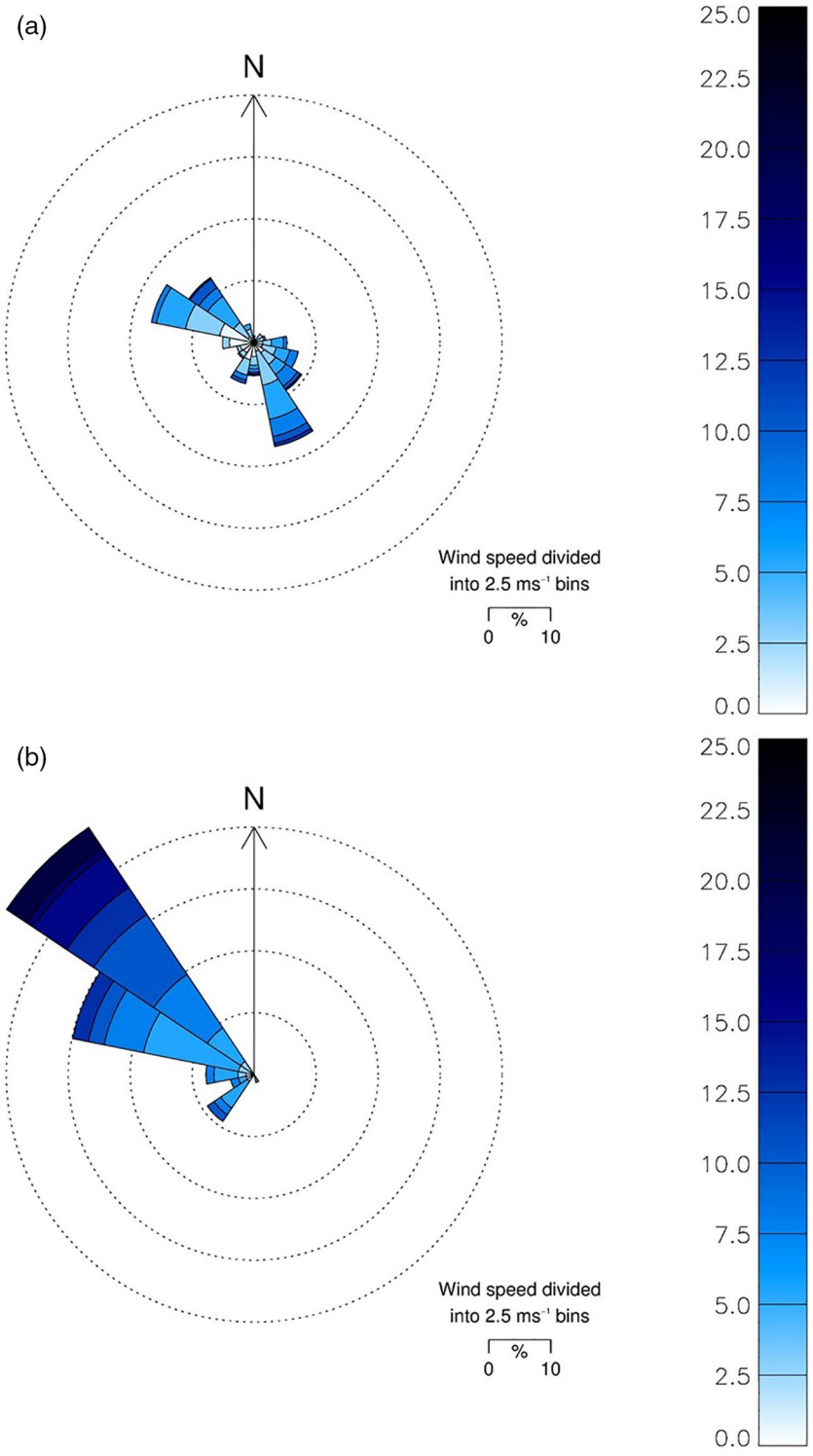

Figure 10. Wind roses for no Föhn (a) and Föhn (b) at the Avery Plateau AWS. AWS, Automatic Weather Station.

For example, the difference in T between Föhn and non-Föhn conditions of about 3 K can be attributed to this change in dd.

Interestingly, the highest temperature at AV (−1.6 °C) is observed on February 7, a time that is not identified as Föhn at CP. At CP, the temperature at this time is −5.3 °C, i.e., 3.7 K lower than at AV. We observe

Table 5
Mean Potential Temperature (K) and Absolute Humidity (g/m^3) for Föhn and no Föhn at Cole Peninsula and Avery Plateau

	Cole Peninsula		Avery Plateau	
	Föhn	No Föhn	Föhn	No Föhn
Potential temperature (K)	277.8	260.7	279.7	277.1
Absolute humidity (g/m^3)	2.2	2.9	2.1	1.7

Northwesterly wind at AV at this time, which would usually indicate Föhn. It is likely that this event was weak in comparison to the stratification over the LCIS, was therefore not able to replace the cold air at the foot of the mountains, and thus did not lead to a Föhn signature in the observations at CP.

The mean difference in the potential temperature at AV and CP is 16 K during no Föhn and 2 K during Föhn. The absolute humidity differs by −0.1 g/m^3 between AV and CP during Föhn and by −1.1 g/m^3 during no Föhn. For clarity values of potential temperature and absolute humidity at these AWSs for Föhn and no Föhn are also presented in Table 5. Both findings indicate that air from the crest of the AP at AV descends down to CP undergoing adiabatic warming during Föhn. This is confirmed by composite cross sections of potential temperature and absolute humidity along 66.8°S using AMPS for no Föhn and Föhn conditions, respectively, which are shown in Figure 11. The blocking effect of the AP during no Föhn is clearly visible, as is the drawdown effect during Föhn conditions. The cross section of potential temperature indicates that Föhn air at CP generally originates from a layer between 1,000 and 1,500 m. The cross section of absolute humidity suggests that Föhn air originates from a layer between 1,500 and 2,000 m. This discrepancy may reflect that Föhn air potentially loses some moisture due to precipitation when ascending on the windward side of the AP. Figure S1, which shows the difference in precipitation (in mm/day) between days with Föhn and days without Föhn, supports this. The air will initially cool at the dry adiabatic lapse rate during its ascent until it reaches saturation. If it rises further, humidity within the air will condensate, and clouds will form. Further ascending the air will now cool at the wet adiabatic lapse rate. The condensed humidity can precipitate out, and thus reduce the absolute humidity of the air. This can explain why the cross section of absolute humidity (Figure 11d) indicates that the Föhn air originates from a higher level than the cross section of potential temperature (Figure 11b).

4.3. Upstream Conditions During Föhn Analyzed Using the Froude Number

We will use the Froude number to characterize the flow conditions upstream of the AWS at CP. This enables us to determine whether the Föhn events we are observing at CP are of linear or nonlinear type. Elvidge and Renfrew (2016) and Orr et al. (2008) show that the upstream flow has a significant influence on the occurrence and characteristics of Föhn events to the east of the AP mountains. The nondimensional Froude number Fr, defined by

$$\mathrm{Fr} = U / NH \tag{1}$$

is often used to describe the upstream conditions. In Equation 1, H is the height of the mountain barrier, and U and N are, respectively, the component of wind perpendicular to the mountain barrier and the Brunt-Vaisala frequency, which are both characteristics of the undisturbed flow upstream of the barrier. When Fr is small, we observe isentropic drawdown, i.e., the westerly upstream flow is predominantly blocked by the AP, and only the uppermost portion of the upwind flow is able to pass over the barrier. In such a case, the air will warm adiabatically as it descends, and lead to a warm, dry Föhn wind over the lee slopes. With increasing Fr, air from lower levels upstream is able to flow over the barrier. At some critical Froude number, $\mathrm{Fr_c}$, the flow transitions from a "nonlinear" (or partially blocked) to a "linear" (or "flow over") regime. Both flow regimes can lead to cross barrier warming, but the patterns of the warming on the LCIS will differ (Elvidge et al., 2016). Nonlinear Föhn are often observed in connection with mountain wave breaking. The subsequent accelerated downslope flow leads to strong warming in the immediate lee of the AP; however, this warming quickly decreases downwind. In cases of linear flow Föhn winds are able to flow at low levels across the entire ice shelf, mechanically mixing the near-surface flow, preventing the development of a strong surface inversion and delivering relatively large fluxes of sensible heat to the ice shelf. This leads to greater potential for higher temperatures and melt over large areas of the LCIS.

For this study, Fr is calculated upwind of CP at 66.8°S, 70°W, using AMPS data at 200 and 2,000 m (Elvidge et al., 2016; King et al., 2017). Following King et al. (2017) we here define $0.2 \leq \mathrm{Fr} < 0.4$ for nonlinear Föhn and $\mathrm{Fr} \geq 0.4$ as linear Föhn. The average Fr during Föhn events is Fr = 0.3, during no Föhn Fr = 0.1. Of 224 Föhn, events 73 are classified as nonlinear, 47 as linear Föhn events. For 64 cases, Fr is <0.2.

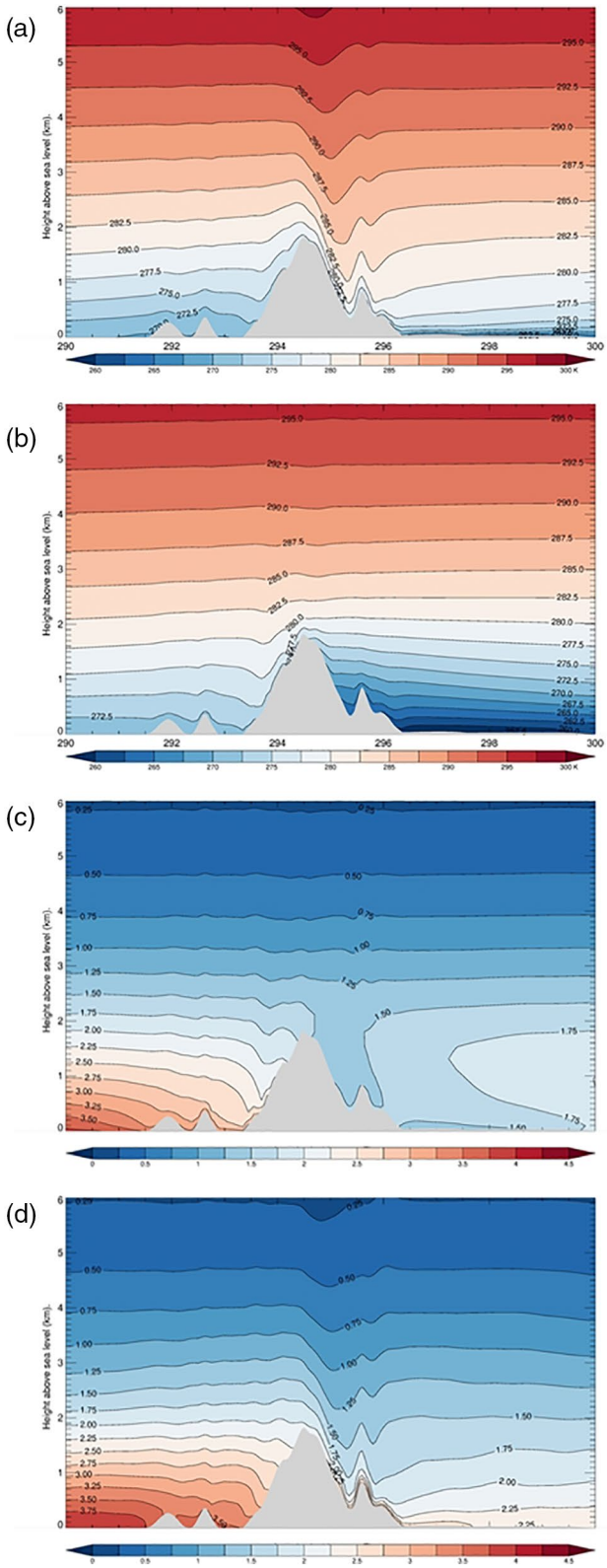

Figure 11. Potential temperature (K) (a), (b) and absolute humidity (g/m^3) (c), (d) cross section along 66.8°S of a composite of no Föhn (a), (c) and Föhn (b), (d) using AMPS data. The composites cover the period during which CP and AV AWS were in operation. AMPS, Antarctic Mesoscale Prediction System; CP, Cole Peninsula; AV, Avery Plateau; AWS, Automatic Weather Station.

The higher proportion of nonlinear Föhn events may explain the strong melt signal reported, e.g., by Luckman et al. (2014) in the far west of the LCIS at the foot of the AP mountains.

The average Fr for the February case introduced above is 0.44, with values ranging from 0.02 to 0.92. This indicates that this is a predominantly linear Föhn case, with less pronounced warming which can spread widely over the LCIS. The average Fr for the August case (0.38) is slightly lower and, with a range from 0.18 to 0.54, is far more consistent than during the February case. This may indicate a more nonlinear Föhn with the strongest warming near the AP and a weakening Föhn signal further east on the LCIS.

Analysis of composites for Föhn of the flow fields near the surface and above the crest of the AP, respectively, have shown that the near-surface flow divides into a northward flow in the northern part of the AP, and (weak) westerly flow further south (Figure 12a). This flow division, caused by the blocking at low level, does not appear higher up (Figure 12b). This indicates that in the northern section (which includes the area this study focusses on), the majority of Föhn cases are of nonlinear nature rather than linear according to the classification by Elvidge and Renfrew (2016). This agrees with the proportion of linear and nonlinear Föhn according to Fr categorization as presented above. The equivalent plots for non-Föhn composites are provided as Supplementary Material (Figure S2).

5. Conclusions

We have presented the analysis of one year of meteorological measurements at an AWS on CP with regard to the occurrence of Föhn, and how characteristics at the location differ during Föhn from the normal state. The analysis found that Föhn conditions occur all year round. Föhn at this location is often short lived, but can persist for up to 4 days.

Throughout the year T and RH values during Föhn events are very similar independent of the season. Taking only non-Föhn into account, they show a clear annual cycle, though.

The average temperature during Föhn is −0.4 °C and RH is 46%. We have shown that Föhn can lead to above freezing air temperature at the location of the AWS even in winter.

We find that on average our measurements at CP compare well with conditions at FG as presented by Cape et al. (2015). Föhn conditions though are weaker at FG than at CP. This is likely a reflection of the fact that the AP mountains are less high windward of FG than windward of CP.

We have shown that the meteorological conditions during Föhn events do not differ significantly throughout the seasons. As a consequence, the relative signal of Föhn events in winter is a lot stronger than in summer. In cases of nonlinear Föhn this is easily explained. In these cases, the Föhn air originates from a level comparable to AV, where the mean June temperature is 5 K higher than at CP, despite being about 1,200 m higher.

Under linear flow, the Föhn air will originate from closer to the surface than under nonlinear flow. In these cases, it is the relatively mild and humid maritime air on the windward side of the AP that adds to the relative strength of Föhn in winter months by the time it reaches the dry and cold conditions at the foot of the AP on the lee side.

Generally, the circulation pattern and the polar vortex favor strong circumpolar westerlies in winter, and thus this is also the season when one would expect most Föhn events to occur. Superimposed on this annual cycle, an increase in the occurrence of Föhn is hypothesized by Orr et al. (2008) for summer. They attribute this to an increase in the Southern Annular Mode, an index describing a pressure pattern that acts to strengthen circumpolar westerly winds. Marshall et al. (2006) determined a significant positive trend in SAM in summer and autumn. For these and logistical reasons, publications have mostly concentrated on Föhn in summer and its relevance to melt on the LCIS (King et al., 2015, 2017; Luckman et al., 2014; van Lipzig et al., 2008). As the temperature signal associated with Föhn can be completely masked by high air temperatures over the LCIS in summer, an increase in Föhn events during this season may not change melt on the ice shelf significantly. The large temperature anomalies in winter due to Föhn seen in Figures 2 and 3, should encourage an increased focus on the role of winter time Föhn events, as is already shown by Kuipers Munneke et al. (2018) and Jakobs et al. (2020).

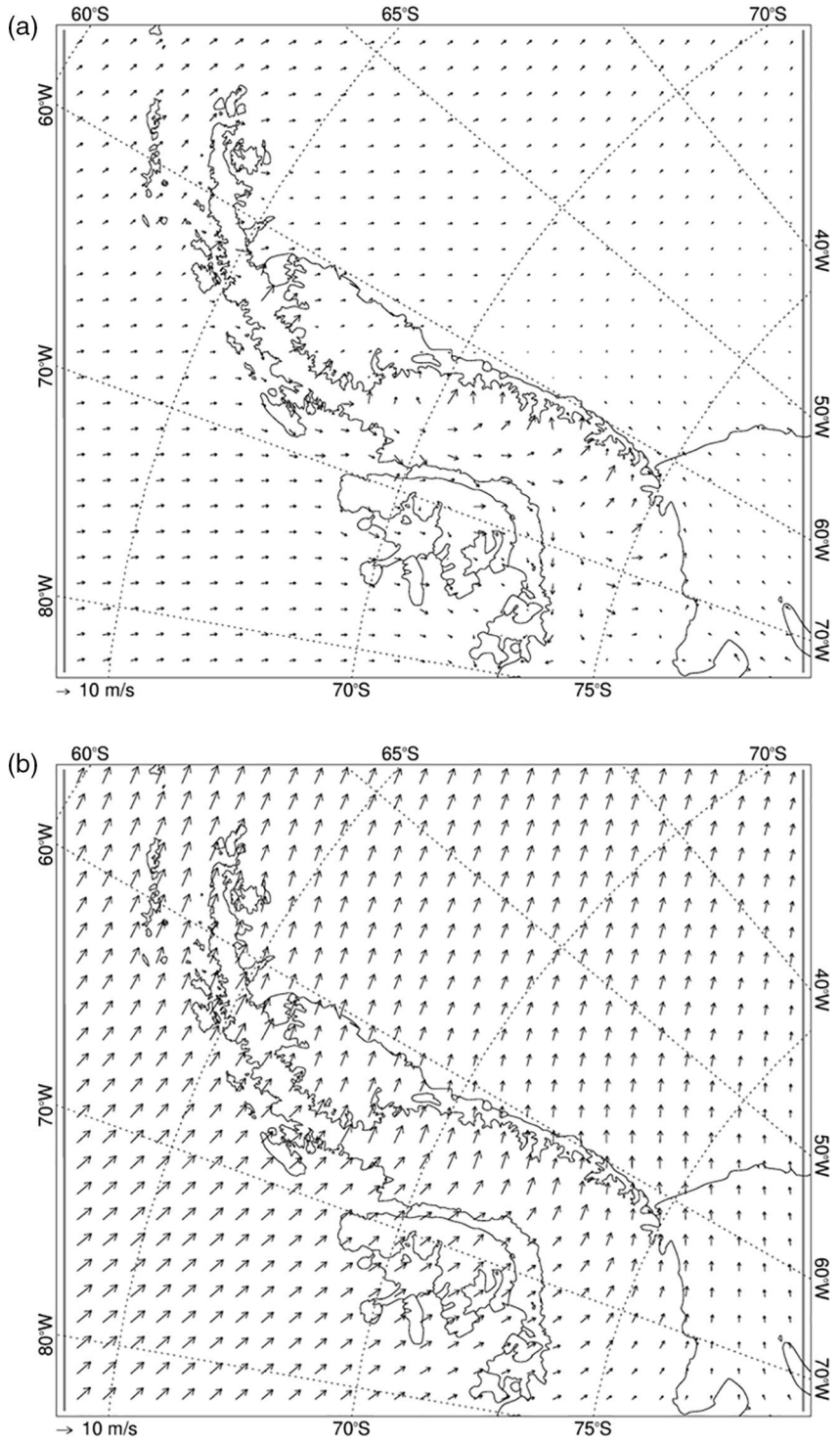

Figure 12. AMPS wind fields for Föhn composites on the lowest model level (1.6 + 0.9984 × p_{sfc} Pa) (a) and above the crest of the AP on hybrid level 17 (244.15 + 0.75585 × p_{sfc} Pa) (b). AMPS, Antarctic Mesoscale Prediction System; AP, Antarctic Peninsula.

Our analysis of the upwind flow conditions reveals that the majority of Föhn is of nonlinear type. In the case of nonlinear Föhn air is sourced from higher altitude upwind of the obstacle as a result of upwind flow blocking at a level below the ridge crest. This type of flow often leads to mountain wave breaking. The con-

nected accelerated downslope wind promotes a strong warming signal directly in the lee of the AP, which does not propagate further across the LCIS.

Potential melt in winter near the AP could precondition the snow and ice surface through firn densification for more efficient melt in spring and summer. This in combination with the fact that the majority of Föhn are nonlinear will contribute significantly to the findings by Luckman et al. (2014) who find the strongest melt signal right at the foot of the AP mountains. The case studies for Föhn in February and August show, that the mechanisms/synoptic situations leading to Föhn in the area covered by this study can be independent of the position of the Amundsen Sea Low and the SAM. The example of a Föhn event in July 2017 that led to the eventual break off of the iceberg A68 from the LCIS (http://www.projectmidas.org/blog/calving/) is a further indication that winter time Föhn events can have significant consequences, and thus warrant further investigation.

As we have found, during Föhn air approaches the AP often from northwesterly directions, before ascending the AP mountains. When the air reaches the condensation level, clouds will form, and precipitation may develop. The Ukrainian Station Vernadsky lies in this area to the northwest of the AP in line with the northern end of the remains of Larsen B ice shelf. Two studies of synoptic observations at the station have studied cloud cover and precipitation between 1960 and 1999. According to Kirchgäßner (2010) total cloud cover at Vernadsky has increased, likely caused by increased amount of high or medium level cloud. This observed trend is strongest (and significant) in winter. Additionally, Kirchgäßner (2011) found a significant increase in precipitation events in winter, and an increase in days with precipitation especially in winter and autumn at Vernadsky over the same period. Both findings are consistent with an increased occurrence of Föhn in winter, and are a further indicator for the importance of Föhn in winter.

Data Availability Statement

Observational data from Cole Peninsula and Avery Plateau can be accessed through the Centre for Environmental Data Analysis (https://catalogue.ceda.ac.uk/uuid/76f82001334afceadfe0df6e1544d75d). The data from Flask Glacier are available to download from https://www.unavco.org/data/gps-gnss/data-access-methods/dai2/app/dai2.html#4Char=FLSK;scope=Station;sampleRate=normal;hasMet=true;4CharMod=startsWith

Acknowledgments
The work reported in this paper was supported by the UK Natural Environment Research Council (NERC) under Grant NE/G014124/1 "Orographic Flows and the Climate of the Antarctic Peninsula." Also a big Thank You to the team at Rothera for help with deployment, maintenance, and recovery of the AWSs at Cole Peninsula and Avery Plateau.

References

Banwell, A. F., MacAyeal, D. R., & Sergienko, O. V. (2013). Break-up of the Larsen B ice shelf triggered by chain-reaction drainage of supraglacial lakes. *Geophysical Research Letters*, *40*, 5872–5876. https://doi.org/10.1002/2013GL057694

Beran, D. W. (1967). Large amplitude Lee waves and Chinook winds. *Journal of Applied Meteorology*, *6*, 865–877.

Cape, M. R., Vernet, M., Skvarca, P., Marinsek, S., Scambos, T., & Domack, E. (2015). Foehn winds link climate-driven warming to ice shelf evolution in Antarctica. *Journal of Geophysical Research: Atmospheres*, *120*, 11037–11057. https://doi.org/10.1002/2015JD023465

Dee, D. P., Uppala, S. M., Simmons, A. J., Berrisford, P., Poli, P., Kobayashi, S., et al. (2011). The ERA-Interim reanalysis: Configuration and performance of the data assimilation system. *Quarterly Journal of the Royal Meteorological Society*, *137*, 553–597.

Draxler, R. R., & Hess, G. D. (1998). An overview of the HYSPLIT_4 modelling system for trajectories, dispersion on and deposition. *Australian Meteorological Magazine*, *47*(4), 295–308.

Elvidge, A. D., & Renfrew, I. A. (2016). The causes of Foehn warming in the Lee of mountains. *Bulletin of the American Meteorological Society*, *97*, 455–466.

Elvidge, A. D., Renfrew, I. A., King, J. C., Orr, A., & Lachlan-Cope, T. A. (2016). Foehn warming distributions in nonlinear and linear flow regimes: A focus on the Antarctic Peninsula. *Quarterly Journal of the Royal Meteorological Society*, *142*, 618–631.

Elvidge, A. D., Renfrew, I. A., King, J. C., Orr, A., Lachlan-Cope, T. A., Weeks, M., & Gray, S. L. (2015). Foehn jets over the Larsen C ice shelf, Antarctica. *Quarterly Journal of the Royal Meteorological Society*, *141*, 698–713.

Fogt, R. L., & Bromwich, D. H. (2008). Atmospheric moisture and cloud cover characteristics forecast by AMPS. *Weather and Forecasting*, *23*, 914–930.

Hann, J. (1885). Einige Bemerkungen zur Entwickelungs-Geschichte der Ansichten über den Ursprung des Föhn (Some remarks about the development of views on the origin of the foehn). *Meteorologische Zeitschrift*, *2*, 393–399.

Hines, K. M., & Bromwich, D. H. (2008). Development and testing of polar weather research and forecasting (WRF) model. Part I: Greenland ice sheet meteorology. *Monthly Weather Review*, *136*, 1971–1989.

Hines, K. M., Bromwich, D. H., Wang, S. H., Silber, I., Verlinde, J., & Lubin, D. (2019). Microphysics of summer clouds in Central West Antarctica simulated by polar WRF and AMPS. *Atmospheric Chemistry and Physics Discussions*, *19*, 12431–12454.

IPCC. (2007). In S. Solomon, D. Qin, M. Manning, Z. Chen, M. Marquis, K.B. Averyt et al. (Eds.), *Climate change 2007: The physical science basis. Contribution of working group I to the fourth assessment report of the intergovernmental panel on climate change* (pp. 996). Cambridge, UK and New York, NY: Cambridge University Press.

Jakobs, C. L., Reijmer, C. H., Smeets, C. J. P. P., Trusel, L. D., van de Berg, W. J., van den Broeke, M. R., & van Wessem, J. M. (2020). A benchmark dataset of in situ Antarctic surface melt rates and energy balance. *Journal of Glaciology*, *66*, 291–302.

King, J. C., Gadian, A., Kirchgaessner, A., Kuipers Munneke, P., Lachlan-Cope, T. A., Orr, A., et al. (2015). Validation of the summertime surface energy budget of Larsen C Ice Shelf (Antarctica) as represented in three high-resolution atmospheric models. *Journal of Geophysical Research: Atmospheres*, *120*, 1335–1347. https://doi.org/10.1002/2014JD022604

King, J. C., Kirchgaessner, A., Bevan, S., Elvidge, A. D., Kuipers Munneke, P., Luckman, A., et al. (2017). The impact of Föhn winds on surface energy balance during the 2010-11 melt season over Larsen C Ice Shelf, Antarctica. *Journal of Geophysical Research: Atmospheres*, *122*, 12062–12076. https://doi.org/10.1002/2017JD026809

King, J. C., Turner, J., Marshall, G. J., Connolley, W. M., & Lachlan-Cope, T. A. (2003). Antarctic Peninsula climate variability and its causes as revealed by analysis of instrumental records. *Antarctic Research Series*, *79*, 17–30.

Kirchgäßner, A. (2010). An analysis of cloud observations from Vernadsky, Antarctica. *International Journal of Climatology*, *30*, 1431–1439.

Kirchgäßner, A. (2011). An analysis of precipitation data from the Antarctic base Faraday/Vernadsky. *International Journal of Climatology*, *31*, 404–414.

Kirchgaessner, A., King, J., & Gadian, A. (2019). The representation of Föhn events to the east of the Antarctic Peninsula in simulations by the Antarctic mesoscale prediction system. *Journal of Geophysical Research: Atmospheres*, *124*, 13663–13679. https://doi.org/10.1029/2019JD030637

Kuipers Munneke, P., Ligtenberg, S. R. M., Van Den Broeke, M. R., & Vaughan, D. G. (2014). Firn air depletion as a precursor of Antarctic ice-shelf collapse. *Journal of Glaciology*, *60*, 205–214.

Kuipers Munneke, P., Luckman, A. J., Bevan, S. L., Smeets, C. J. P. P., Gilbert, E., van den Broeke, M. R., et al. (2018). Intense winter surface melt on an Antarctic ice shelf. *Geophysical Research Letters*, *45*, 7615–7623. https://doi.org/10.1029/2018GL077899

Kuipers Munneke, P., van den Broeke, M. R., King, J. C., Gray, T., & Reijmer, C. H. (2012). Near-surface climate and surface energy budget of Larsen C ice shelf, Antarctic Peninsula. *The Cryosphere*, *6*, 353–363.

Luckman, A., Elvidge, A. D., Jansen, D., Kulessa, B., Kuipers Munneke, P., King, J. C., & Barrand, N. E. (2014). Surface melt and ponding on Larsen C Ice Shelf and the impact of Föhn winds. *Antarctic Science*, *26*, 625–635.

Marshall, G. J. (2003). Trends in the southern annular mode from observations and reanalyses. *Journal of Climate*, *16*, 4134–4143.

Marshall, G. J. (2004). Causes of exceptional atmospheric circulation changes in the Southern Hemisphere. *Geophysical Research Letters*, *31*. L14205. https://doi.org/10.1029/2004GL019952

Marshall, G. J., Lagun, V., & Lachlan-Cope, T. A. (2002). Changes in Antarctic Peninsula tropospheric temperatures from 1956-1999: A synthesis of observations and reanalysis data. *International Journal of Climatology*, *22*, 291–310.

Marshall, G. J., Orr, A., Lipzig, N. P. M. V., & King, J. C. (2006). The impact of a changing southern hemisphere annular mode on Antarctic Peninsula summer temperatures. *Journal of Climate*, *19*, 5388–5404.

McGrath, D., Steffen, K., Rajaram, H., Scambos, T., Abdalati, W., & Rignot, E. (2012). Basal crevasses on the Larsen C Ice Shelf, Antarctica: Implications for meltwater ponding and hydrofracture. *Geophysical Research Letters*, *39*, L16504. https://doi.org/10.1029/2012GL052413

Ólafsson, H. (2005). The heat source of the foehn. *Croatian Meteorological Journal*, *40*, 542–545.

Orr, A., Cresswell, D., Marshall, G. J., Hunt, J. C. R., Sommeria, J., & Wang, C. G. (2004). A 'low-level' explanation for the recent large warming trend over the Western Antarctic Peninsula involving blocked winds and changes in zonal circulation. *Geophysical Research Letters*, *31*, L06204. https://doi.org/10.1029/2003GL019160

Orr, A., Marshall, G. J., Hunt, J. C. R., Sommeria, J., Wang, C.-G., van Lipzig, N. P. M., et al. (2008). Characteristics of summer airflow over the Antarctic Peninsula in response to recent strengthening of westerly circumpolar winds. *Journal of the Atmospheric Sciences*, *65*, 1396–1413.

Powers, J. G., Manning, K. W., Bromwich, D. H., Cassano, J. J., & Cayette, A. M. (2012). A decade of Antarctic science support through amps. *Bulletin of the American Meteorological Society*, *93*, 1699–1712.

Powers, J. G., Monaghan, A. J., Cayette, A. M., Bromwich, D. H., Kuo, Y.-H., & Manning, K. W. (2003). Real-time mesoscale modeling over Antarctica: The Antarctic mesoscale prediction system. *Bulletin of the American Meteorological Society*, *84*, 1533–1545.

Richner, H., Baumann-Stanzer, K., Benech, B., Berger, H., Chimani, B., Dorninger, M., et al. (2006). Unstationary aspects of foehn in a large valley part I: Operational setup, scientific objectives and analysis of the cases during the special observing period of the MAP subprogramme FORM. *Meteorology and Atmospheric Physics*, *92*, 255–284.

Richner, H., & Hächler, P. (2013). In K. F. Chow, F. J. S. De Wekker, & J. B. Snyder (Eds.), *Understanding and forecasting Alpine Foehn. Mountain weather research and forecasting: Recent progress and current challenges* (pp. 219–260). Netherlands: Springer.

Scambos, T., Hulbe, C., & Fahnestock, M. (2003). Antarctic Peninsula climate variability. *Historical and Paleoenvironmental Perspectives*, *79*, 79–92.

Scambos, T., & Truffer, M. (2010). *Antarctica-PI continuous: FLSK-Flask Glacier P.S., UNAVCO, GPS data set*. Boulder, CO: UNAVCO.

Skamarock, W., Klemp, J., Dudhia, J., Gill, D., Barker, D., Wang, W., et al. (2008). *A description of the advanced research WRF version 3* (Technical Notes NCAR/TN-4751STR, pp. 113). University Corporation for Atmospheric Research.

Smith, R. (1990). Why can't stably stratified air rise over high ground. In *Atmospheric processes over complex terrain* (pp. 105–107). Boston, MA: American Meteorological Society.

Speirs, J. C., Steinhoff, D. F., McGowan, H. A., Bromwich, D. H., & Monaghan, A. J. (2010). Foehn winds in the McMurdo Dry Valleys, Antarctica: The origin of extreme warming events. *Journal of Climate*, *23*, 3577–3598.

Steinhoff, D. F., Bromwich, D. H., Speirs, J. C., McGowan, H. A., & Monaghan, A. J. (2014). Austral summer foehn winds over the McMurdo dry valleys of Antarctica from polar WRF. *Quarterly Journal of the Royal Meteorological Society*, *140*, 1825–1837.

Turner, J., Colwell, S. R., Marshall, G. J., Lachlan-Cope, T. A., Carleton, A. M., Jones, P. D., et al. (2005). Antarctic climate change during the last 50 years. *International Journal of Climatology*, *25*, 279–294.

Turner, J., Lu, H., White, I., King, J. C., Phillips, T., Hosking, J. S., et al. (2016). Absence of 21st century warming on Antarctic Peninsula consistent with natural variability. *Nature*, *535*, 411.

Turton, J. V., Kirchgaessner, A., Ross, A. N., & King, J. C. (2017). Does high-resolution modelling improve the spatial analysis of Föhn flow over the Larsen C ice shelf? *Weather*, *72*, 192–196.

Turton, J. V., Kirchgaessner, A., Ross, A. N., & King, J. C. (2018). The spatial distribution and temporal variability of Föhn winds over the Larsen C ice shelf, Antarctica. *Quarterly Journal of the Royal Meteorological Society*, *144*, 1169–1178.

van Lipzig, N. P. M., Marshall, G. J., Orr, A., & King, J. C. (2008). The relationship between the southern hemisphere annular mode and Antarctic Peninsula summer temperatures: Analysis of a high-resolution model climatology. *Journal of Climate*, *21*, 1649–1668.

Vaughan, D. G., Marshall, G. J., Connolley, W. M., King, J. C., & Mulvaney, R. (2001). Devil in the detail. *Science*, *293*, 1777–1779.

Whiteman, C. D. (2000). *Mountain meteorology: Fundamentals and applications* (355pp). New York and Oxford: Oxford University Press.

Wille, J. D., Bromwich, D. H., Nigro, M. A., Cassano, J. J., Mateling, M., Lazzara, M. A., & Wang, S.-H. (2016). Evaluation of the AMPS boundary layer simulations on the Ross ice shelf with tower observations. *Journal of Applied Meteorology and Climatology*, *55*, 2349–2367.